A Model Predictive Voltage Control using Virtual Space Vectors for Grid-Forming Energy Storage Converters

Waleed Alhosaini
Department of Electrical Engineering
University of Arkansas
Fayetteville, USA
wsalhosa@uark.edu

Yue Zhao
Department of Electrical Engineering
University of Arkansas
Fayetteville, USA
yuezhao@uark.edu

***Abstract*—Sinusoidal output voltages with low harmonic distortion can be achieved using three-level converters along with *LC* filters, which have been proven to be suitable for energy storage systems (ESSs). Model predictive control (MPC) has been applied to such energy storage converters due to its simplicity and effectiveness. However, selecting the weighting factor of the additional neutral-point (NP) voltage balancing term in the cost function is time consuming and may also affect the main objective of MPC. To address this issue, in this paper, additional virtual space vectors (VSVs), which do not affect the NP capacitor voltages, are adopted in the proposed MPC. Both simulation and experimental results using controller hardware-in-the-loop are presented to show that NP capacitor voltages can be well controlled using a particularly small NP voltage balancing weighting factor in the cost function. In addition, the total harmonic distortion of the voltage at the point of common coupling is reduced while retaining the fast dynamic response of MPC.**

Keywords—energy storage system, model predictive control, neutral point voltage, virtual space vector

I. Introduction

The use of energy storage systems (ESSs) as grid forming converters in microgrids (MGs) can significantly improve electrical power systems' reliability [1], [2]. Since more and more distributed energy resources (DERs) are integrated into the modern power system, power electronic technologies as well as advanced control methods have become essential to achieve enhanced power quality with reduced system losses [3], [4].

Considering different high-power multilevel converters such as flying capacitors (FC) converters, cascade H-bridge, and neutral-point clamped (NPC) converters, the latter has been proven to be suitable for wide range of industrial applications [5], [6], which include medium- and high-voltage DER interface [7]. However, one of main challenges related to NPC converters control is the neutral-point (NP) voltage balancing, since in such topology the NP potential may have significant fluctuations [8], [9]. This issue has been addressed in model predictive control (MPC) by adding a term representing the NP voltage in the cost function to minimize the error between the voltage across the two dc-link capacitors and eventually control the dc-link capacitor voltages [10]-[14]. Nevertheless, this additional term may affect the main objective of MPC, and the tuning effort for this weighting factor is time consuming [11].

Thus, in this paper, the virtual space vectors (VSVs) are adopted for the proposed MPC. Using the concept of VSVs for SVPWM was originally presented in [15]. By adopting VSV for MPC, the weighting factor for NP voltage term can be kept low enough while maintaining the voltage balancing between two dc link capacitors. If only VSVs are used in the converter control set, the NP voltage term can even be eliminated from the cost function. Furthermore, with the additional VSVs, the performance of the voltage reference tracking has been improved while the THD of the PCC voltage is decreased. The proposed control scheme achieves all of these improvements without affecting the simplicity of the conventional MPC.

In this paper, both simulation and experimental results using controller hardware in the loop (C-HIL) are presented to show the clear improvement in the MPC performance by introducing a set of six VSVs into the MPC design. The studied system, shown in Fig. 1, consists of an NPC converter, dc-link capacitors, an *LC* filter and a load. The system under investigation is intended to work as a grid forming ESS inverter where it provides power to the load.

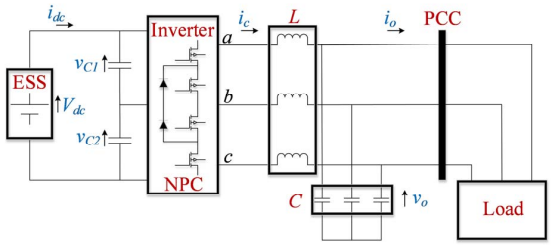

Fig. 1. An overall diagram of the studied system.

II. System Modeling

In this section, the detailed mathematical models of the generic NPC converter, the dc-link capacitors, and the *LC* filter are presented, since these models are critical for the MPC design.

This material is based upon work supported by the U.S. Department of Energy's Office of Energy Efficiency and Renewable Energy (EERE) under the Award Number DE-EE0008349. This work was also supported in part by the U.S. National Science Foundation (NSF) within the Industry/ University Cooperative Research Center (I/UCRC) on Grid Connected Advanced Power Electronic Systems (GRAPES) under Grant IIP-1439700.

A. NPC Converter Model

Fig. 2 depicts the schematic of a generic three-phase three-level NPC inverter. The output voltage space vectors, which are generated by the NPC converter [13], [14] can be expressed as

$$v_i = \frac{2}{3}(v_{ao} + a \cdot v_{bo} + a^2 \cdot v_{co}) \tag{1}$$

where v_{ao}, v_{bo} and v_{co} are the inverter line-to-neutral output voltages and $a = e^{j2\pi/3}$.

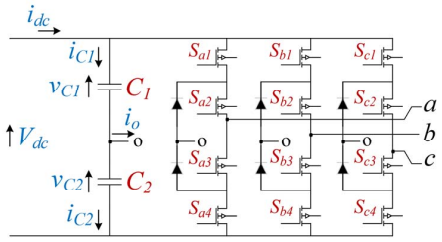

Fig. 2. Schematic of a generic NPC inverter

Assuming the voltages across the dc-link capacitors are balanced, the NPC inverter line-to-neutral output voltages [13], [14] can be expressed as

$$v_{xo} = S_x \frac{V_{dc}}{2} \tag{2}$$

where $V_{dc} = v_{C1} + v_{C2}$, and S_x is the gating signals and $x = \{a, b, c\}$.

For NPC converters, there are 27 voltage space vectors in total, among which there are 19 non-redundant active voltage vectors. Table I summarizes the switching states for phase x, which can be +, 0 and –, and can generate $V_{dc}/2$, 0, and $-V_{dc}/2$, respectively, at the terminal of phase x of NPC converter [13].

TABLE I. THE CONVERTER SWITCHING STATES OF PHASE X

S_x	SS_{x1}	SS_{x2}	SS_{x3}	SS_{x4}	V_{xo}
+	1	1	0	0	$V_{dc}/2$
0	0	1	1	0	0
–	0	0	1	1	$-V_{dc}/2$

B. DC-link Capacitor Model

The dc-link capacitor voltages can be modeled by using the capacitor voltage differential equation [13] as

$$\frac{dv_{C1}}{dt} = \frac{i_{C1}}{C_1} \tag{3}$$

$$\frac{dv_{C2}}{dt} = \frac{i_{C2}}{C_2} \tag{4}$$

where

C_1, C_2 upper and lower dc-link capacitor values;
v_{C1}, v_{C2} dc-link capacitor voltages;
i_{C1}, i_{C2} currents through the dc-link capacitors.

Then, using forward Euler approximation, the discrete-time model of dc-link capacitors [13] can be obtained as

$$v_{C1}(k+1) = v_{C1}(k) + \frac{T_S}{C_1} i_{C1}(k) \tag{5}$$

$$v_{C2}(k+1) = v_{C2}(k) + \frac{T_S}{C_2} i_{C2}(k) \tag{6}$$

where T_s is the sampling period, which also equals to the switching period in this work. The k and $k + 1$ represent two consecutive sampling periods.

The currents flowing through the dc-link capacitors, which are i_{C1} and i_{C2}, are calculated based on the dc-link current supplied by the ESS, i_{dc}, the applied switching states, S_{x1} and S_{x2}, and the measured instantaneous three-phase inverter currents i_a, i_b, and i_c as follows

$$i_{C1}(k) = i_{dc}(k) - H_{1a} i_a(k) - H_{1b} i_b(k) - H_{1c} i_c(k) \tag{7}$$

$$i_{C2}(k) = i_{dc}(k) + H_{2a} i_a(k) + H_{2b} i_b(k) + H_{2c} i_c(k) \tag{8}$$

where

$H_{1x} = 1$ if $S_x =$ "+", otherwise $H_{1x} = 0$;
$H_{2x} = 1$ if $S_x =$ "–", otherwise $H_{2x} = 0$.

C. LC Filter Model

The continuous-time mathematical model of the LC filter, which is expressed in (9), is derived by applying KVL and KCL on the LC filter one-line diagram shown in Fig. 3 [16].

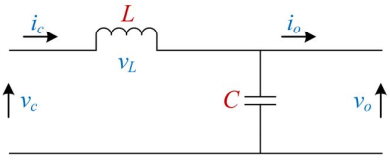

Fig. 3. One-line diagram of the LC filter.

$$\frac{d}{dt}\begin{bmatrix} i_c \\ v_o \end{bmatrix} = \begin{bmatrix} 0 & -\frac{1}{L} \\ \frac{1}{C} & 0 \end{bmatrix}\begin{bmatrix} i_c \\ v_o \end{bmatrix} + \begin{bmatrix} \frac{1}{L} & 0 \\ 0 & -\frac{1}{C} \end{bmatrix}\begin{bmatrix} v_c \\ i_o \end{bmatrix} \tag{9}$$

where

L, C LC filter inductance and capacitance;
v_c, i_c converter side voltage and current;
v_o, i_o PCC side voltage and current.

Then, the discrete-time mathematical form of the LC filter can be obtained using the forward Euler approximation as

$$\begin{bmatrix} i_c(k+1) \\ v_o(k+1) \end{bmatrix} = \begin{bmatrix} 1 & -\frac{T_S}{L} \\ \frac{T_S}{C} & 1 \end{bmatrix}\begin{bmatrix} i_c(k) \\ v_o(k) \end{bmatrix} + \begin{bmatrix} \frac{T_S}{L} & 0 \\ 0 & -\frac{T_S}{C} \end{bmatrix}\begin{bmatrix} v_c(k) \\ i_o(k) \end{bmatrix} \tag{10}$$

III. CONVENTIONAL MODEL PREDICTIVE CONTROL

The flow chart of the conventional model predictive control (MPC) for an NPC inverter with an LC filter is shown in Fig. 4. The values of the converter side current, i_c, the load side current, i_o, the LC filter capacitor voltage, v_o, the ESS current, i_{dc}, and the dc-link capacitor voltages, v_{C1} and v_{C2}, are measured at sampling period k. Using these

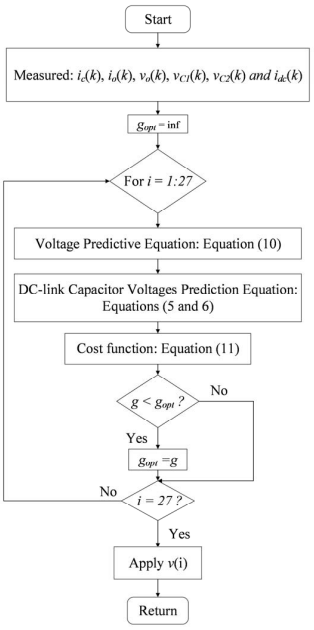

Fig. 4. Flow chart of the Typical MPC.

measurements, the dc-link capacitor voltages, v_{C1} and v_{C2}, and the PCC voltage, v_o, are predicted for the sampling period k+1 using (5), (6) and (10), respectively. The cost function, g, is used to evaluate the 27 voltage space vectors. The optimal voltage vector, v_i, which minimizes g, is applied in the next sampling period, k+1. Since the main objective of the designed MPC is to achieve desired reference voltage tracking at the PCC with acceptable NP voltage oscillations, the cost function, g, is designed as follows

$$g = (v^*_{o,\alpha} - v_{o,\alpha})^2 + (v^*_{o,\beta} - v_{o,\beta})^2 + \lambda_{dc}(v_{C1} - v_{C2})^2 \quad (11)$$

where

$v^*_{o,\alpha}$, $v^*_{o,\beta}$ real and imaginary parts of the reference voltage, v^*_o;

$v_{o,\alpha}$, $v_{o,\beta}$ real and imaginary parts of the predicted PCC voltage at sampling period k+1;

v_{C1}, v_{C2} predicted dc-link capacitor voltages at sampling period k+1;

λ_{dc} weighting factor for the NP voltage balancing term.

IV. The Proposed MPC using Virtual Space Vectors

Over one switching cycle, T_s, if the average NP current, which is i_o shown in Fig. 2, is not zero in an NPC converter, the NP voltage oscillation will occur [17]. To address this issue, the concept of virtual space vectors (VSVs) was introduced in [15] and implemented for SVPWM approach. The VSVs are a set of space vectors synthesized by using three original voltage space vectors, e.g., V_x, V_y, and V_z shown in Table II, however, the resulting i_o is zero over a switching period, when any of the VSV is applied. Following this concept, in this paper, six VSVs, shown in Fig. 6(a), are added to the NPC converter control set. Their associated average NP current, i_o, over a switching cycle, T_s, is equal to zero. Using the VSV V_{v1} as an example, V_{v1} is synthesized as

$$V_{v1} = (V_1 + V_2 + V_8)/3 \quad (15)$$

In this proposed technique, the extended switching states of an original voltage space vector V_m (m = 1, 1, 2, … , 19) is defined using the form of

$$SS^*_m = (SS_{a1}\ SS_{a2}\ SS_{b1}\ SS_{b2}\ SS_{c1}\ SS_{c2}) \quad (16)$$

Then, the extended switching states for V_{v1} can be easily determined as

$$SS^*_{v1} = (SS^*_1 + SS^*_2 + SS^*_8)/3$$
$$= \left(\frac{0+1+1}{3}\ \frac{1+1+1}{3}\ \frac{0+0+1}{3}\ \frac{0+1+1}{3}\ \frac{0+0+0}{3}\ \frac{0+0+1}{3}\right)$$
$$= \left(\frac{2}{3}\ 1\ \frac{1}{3}\ \frac{2}{3}\ 0\ \frac{1}{3}\right) \quad (17)$$

All the extended switching states for VSVs are summarized in Table II. Using the extended switching states, VSVs as well as the original voltage space vectors are mapped to the switching gate signals using an external modulator as presented in the MPC based VSVs control block diagram shown in Fig. 5. This modulator compares the extended switching states of the optimal voltage vector selected by MPC algorithm with a carrier waveform which has a fixed switching frequency. An example to generate gate signals for V_{v1} is shown in Fig. 6(b).

TABLE II. A Summary of the Extended Switching States of VSVs

VSV	V_x	SS of V_x	V_y	SS of V_x	V_z	SS of V_z	*Extended Switching States of VSVs*					
							S_{a1}	S_{a2}	S_{b1}	S_{b2}	S_{c1}	S_{c2}
V_{v1}	V_1	(0, –, –)	V_2	(+, +, 0)	V_8	(+, 0, –)	2/3	1	1/3	2/3	0	1/3
V_{v2}	V_2	(+, +, 0)	V_3	(–, 0, –)	V_{10}	(0, +, –)	1/3	2/3	2/3	1	0	1/3
V_{v3}	V_3	(–, 0, –)	V_4	(0, +, +)	V_{12}	(–, +, 0)	0	1/3	2/3	1	1/3	2/3
V_{v4}	V_4	(0, +, +)	V_5	(–, –, 0)	V_{14}	(–, 0, +)	0	1/3	1/3	2/3	2/3	1
V_{v5}	V_5	(–, –, 0)	V_6	(+, 0, +)	V_{16}	(0, –, +)	1/3	2/3	0	1/3	2/3	1
V_{v6}	V_6	(+, 0, +)	V_1	(0, –, –)	V_{18}	(+, –, 0)	2/3	1	0	1/3	1/3	2/3

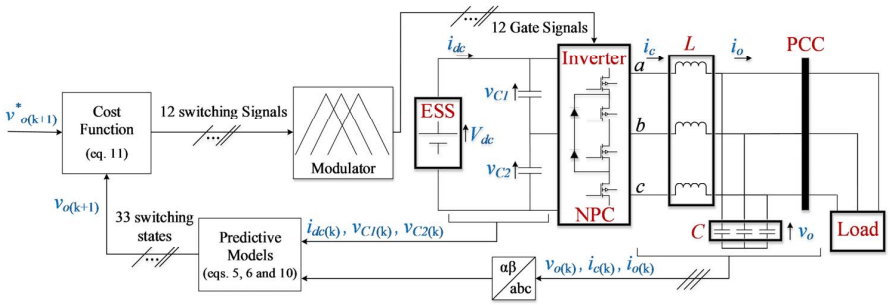

Fig. 5. Control block diagram of the proposed MPC based VSVs.

The use of VSVs generates zero average NP current over a switching cycle, such that NP voltage is not affected. Therefore, if VSVs are added into the space vector voltage set, the NP voltage oscillation issue will be mitigated. Additionally, as more space vectors are used, the THD_v at the PCC is noticeably reduced. If only VSVs are used, the NP voltage unbalancing issue can be addressed inherently, even eliminating the need of using any NP voltage balancing term in the cost function. Finally, MPC based VSVs algorithm has to be updated since the number of the voltage vectors which needs to be evaluated in the cost function increased from 27 to 33 voltage vectors. The flow chart of the algorithm of the proposed MPC is shown in Fig. 7.

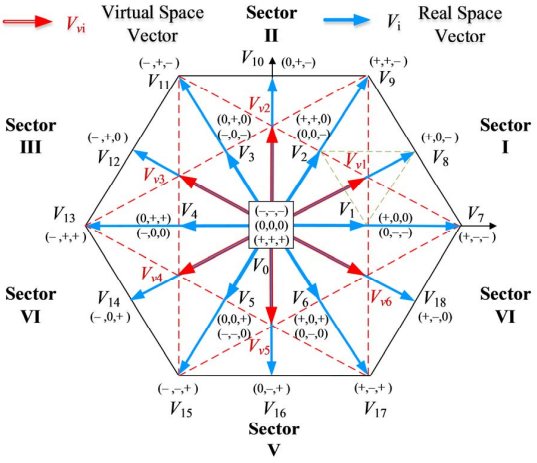

(a)

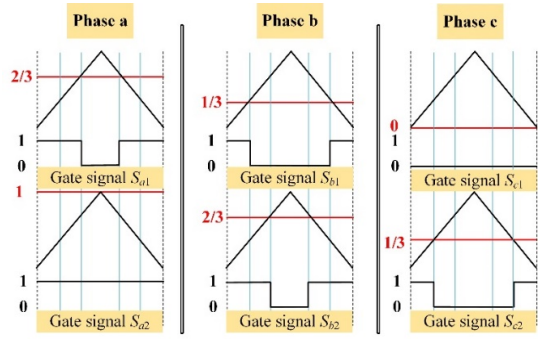

(b)

Fig. 6. (a) Space vector diagram of an NPC inverter with the virtual voltage vectors (VSVs) included, (b) Generation of switch gate signals of V_{v1} using a modulator.

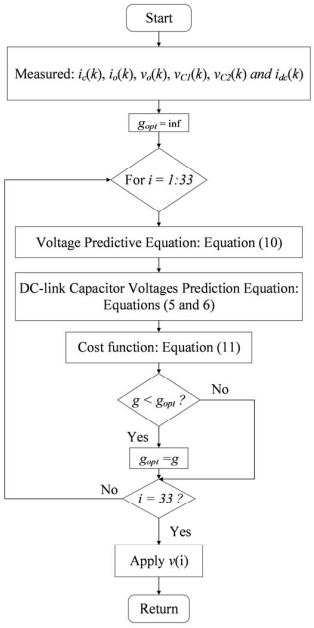

Fig. 7. Flow chart of the proposed MPC based VSVs.

V. Simulation Studies

Simulation studies are performed using MATLAB Simulink and the results presented in this paper. Considering the conventional MPC, as shown in Fig. 6, the simulation started using a NP voltage-balancing weighting factor, λ_{dc}, which is equal to 2.5. At t = 3.0 s, λ_{dc} has been reduced to become only 0.05. The dc-link capacitor voltages diverges as soon as λ_{dc} changed to 0.05. Then, the six VSVs are introduced into the space vector set at t = 6.0 s while λ_{dc} is maintained at the value of 0.05 to analyze the impact of the VSVs on the NP capacitor voltage. It can be clearly observed the dc-link capacitor voltages start to converge once the VSVs are activated.

The use of the VSVs into the converter control set has also enhanced the PCC voltage quality as demonstrated in Fig. 7. Using the typical MPC with λ_{dc} = 2.5 provides three-phase output voltage at the PCC with THD_v = 2.15 % as shown in Fig. 7(a). If λ_{dc} is reduced to 0.05, the THD_v, displayed in Fig. 7(b), increases to 2.45 % due to the divergence in the dc-link capacitor voltages. However, adopting the proposed control method allows to achieve THD_v at the PCC voltage as low as 1.70 % with λ_{dc} = 0.05. The PCC voltage is also compared with the reference voltage in dq0-rotating frame considering the conventional

MPC with λ_{dc} = 2.5, the conventional MPC with λ_{dc} = 0.05 and the proposed MPC with λ_{dc} = 0.05 as shown in Fig. 8. The proposed MPC has shown less voltage ripple in the PCC output voltage compared to the classical MPC when λ_{dc} = 0.05.

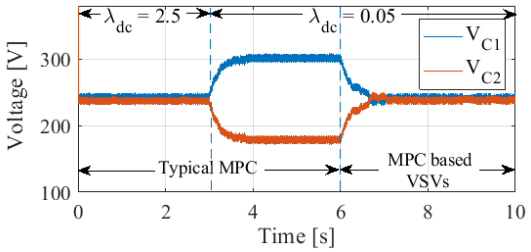

Fig. 6. DC-link capacitor voltages.

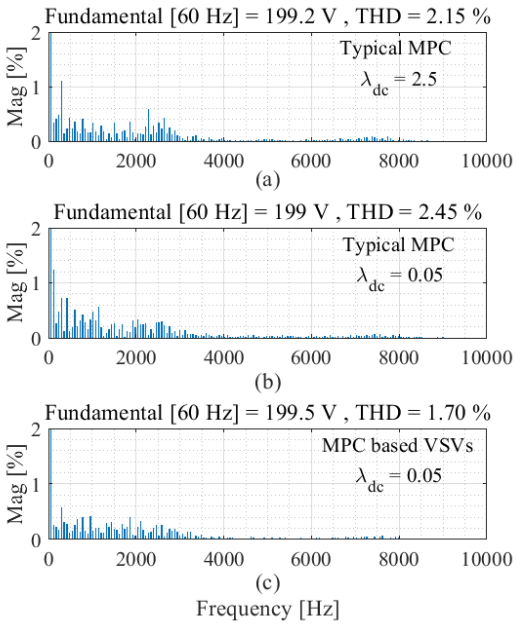

Fig. 7. PCC voltage spectrums.

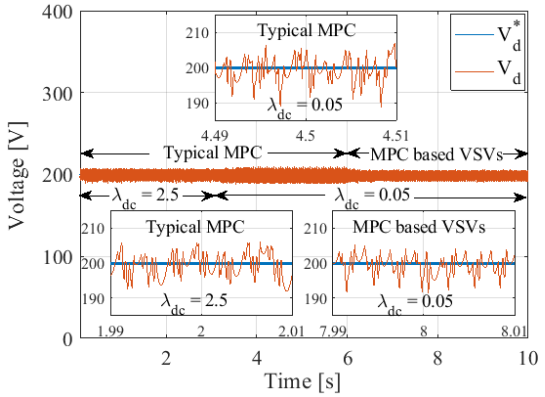

Fig. 8. PCC reference and actual voltage in dq0-rotating frame.

VI. Experimental Studies

The validity of the simulation studies has been confirmed using C-HIL. The proposed controller was implemented using dSPACE DS1202 while the investigated system was modeled and implemented Typhoon HIL 602+.

As demonstrated in Fig. 9, the NP capacitor voltages are balanced when a large enough weighting factor, i.e. λ_{dc} = 2.5, is used when the classical MPC applied. However, once λ_{dc} is selected to be 0.05 at t = 3.0 s, NP voltage divergence occurred. On the other hand, implementing the proposed MPC at t = 7.0 s allows to maintain the dc-link capacitor voltages balanced although a substantially weighting factor, i.e. λ_{dc} = 0.05, is considered.

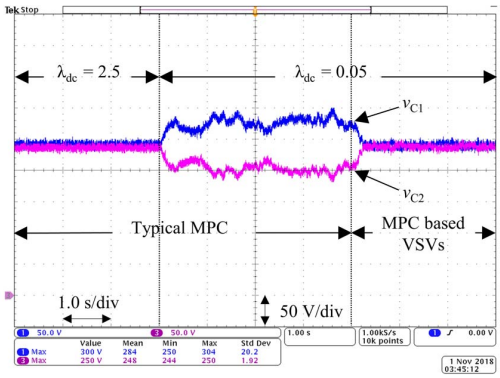

Fig. 9. DC-link capacitor voltages.

The THD_v of the PCC three-phase voltage is also analyzed and compared when both the typical MPC and MPC based VSVs are used. Fig. 10(a) shows using a sufficient large weighting factor, i.e. λ_{dc} = 2.5, in the conventional MPC has led THD_v = 1.04 %. The THD_v has been increased by 0.60 % when λ_{dc} = 0.05 as explained in Fig. 10(b). Nevertheless, the implementation of the proposed MPC has improved the PCC voltage quality. Fig. 10(c) demonstrates that the use of the VSVs in the inverter control set leads to have THD_v = 0.87 %.

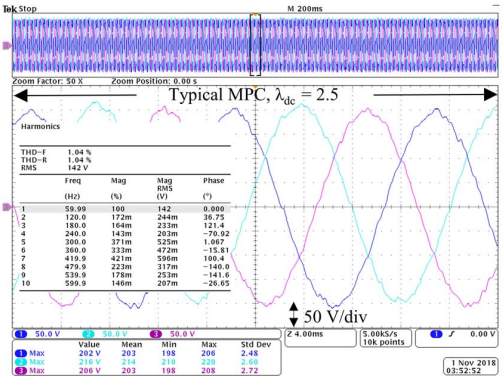

(a)

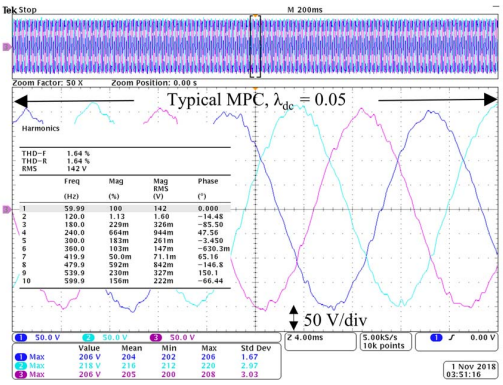

(b)

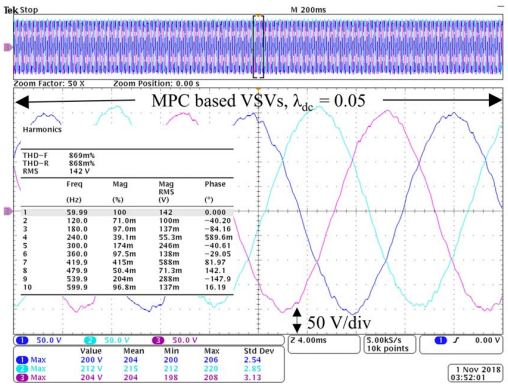

(c)

Fig. 10. Three-phase voltage at the PCC, (a) Conventional MPC with λ_{dc} = 2.5, (b) Conventional MPC with λ_{dc} = 0.05, (c) Proposed MPC based VSVs with λ_{dc} = 0.05.

VII. Conclusions

In this work, an improved MPC method is presented for three-phase three-level NPC converters with output *LC* filters. A set of six VSVs are adopted into the MPC design. These VSVs allow using a considerably small weighting factor, λ_{dc}, for the NP voltage-balancing term in the cost function. As a result, the main objective of the designed MPC becomes the output voltage reference tracking. Furthermore, the THD_v of the PCC voltage has been reduced as more voltage vectors introduced into the converter control set. Simulation and C-HIL results show the effectiveness of the presented control approach.

References

[1] M. A. Abusara, J. M. Guerrero and S. M. Sharkh, "Line-Interactive UPS for Microgrids," in *IEEE Transactions on Industrial Electronics*, vol. 61, no. 3, pp. 1292-1300, March 2014.

[2] J. M. Guerrero, J. C. Vasquez, J. Matas, L. G. de Vicuna and M. Castilla, "Hierarchical Control of Droop-Controlled AC and DC Microgrids—A General Approach Toward Standardization," in *IEEE Transactions on Industrial Electronics*, vol. 58, no. 1, pp. 158-172, Jan. 2011.

[3] H. Abu-Rub, J. Holtz, J. Rodriguez and G. Baoming, "Medium-Voltage Multilevel Converters—State of the Art, Challenges, and Requirements in Industrial Applications," in *IEEE Transactions on Industrial Electronics*, vol. 57, no. 8, pp. 2581-2596, Aug. 2010.

[4] F. Blaabjerg, Zhe Chen and S. B. Kjaer, "Power electronics as efficient interface in dispersed power generation systems," in *IEEE Transactions on Power Electronics*, vol. 19, no. 5, pp. 1184-1194, Sept. 2004.

[5] J. Rodriguez, S. Bernet, P. K. Steimer and I. E. Lizama, "A Survey on Neutral-Point-Clamped Inverters," in *IEEE Transactions on Industrial Electronics*, vol. 57, no. 7, pp. 2219-2230, July 2010.

[6] J. Pou, J. Zaragoza, S. Ceballos, M. Saeedifard and D. Boroyevich, "A Carrier-Based PWM Strategy With Zero-Sequence Voltage Injection for a Three-Level Neutral-Point-Clamped Converter," in *IEEE Transactions on Power Electronics*, vol. 27, no. 2, pp. 642-651, Feb. 2012.

[7] Y. Jiao, F. C. Lee and S. Lu, "Space Vector Modulation for Three-Level NPC Converter With Neutral Point Voltage Balance and Switching Loss Reduction," in *IEEE Transactions on Power Electronics*, vol. 29, no. 10, pp. 5579-5591, Oct. 2014.

[8] W. Song, X. Feng and K. M. Smedley, "A Carrier-Based PWM Strategy With the Offset Voltage Injection for Single-Phase Three-Level Neutral-Point-Clamped Converters," in *IEEE Transactions on Power Electronics*, vol. 28, no. 3, pp. 1083-1095, March 2013.

[9] H. Chen, M. Tsai, Y. Wang and P. Cheng, "A novel neutral point potential control for the three-level neutral-point-clamped converter," *2016 IEEE Energy Conversion Congress and Exposition (ECCE)*, Milwaukee, WI, 2016, pp. 1-7.

[10] V. Yaramasu, B. Wu, S. Alepuz and S. Kouro, "Predictive Control for Low-Voltage Ride-Through Enhancement of Three-Level-Boost and NPC-Converter-Based PMSG Wind Turbine," in *IEEE Transactions on Industrial Electronics*, vol. 61, no. 12, pp. 6832-6843, Dec. 2014.

[11] F. Donoso, A. Mora, R. Cárdenas, A. Angulo, D. Sáez and M. Rivera, "Finite-Set Model-Predictive Control Strategies for a 3L-NPC Inverter Operating With Fixed Switching Frequency," in *IEEE Transactions on Industrial Electronics*, vol. 65, no. 5, pp. 3954-3965, May 2018.

[12] P. Acuña, L. Morán, M. Rivera, R. Aguilera, R. Burgos and V. G. Agelidis, "A Single-Objective Predictive Control Method for a Multivariable Single-Phase Three-Level NPC Converter-Based Active Power Filter," in *IEEE Transactions on Industrial Electronics*, vol. 62, no. 7, pp. 4598-4607, July 2015.

[13] A. Calle-Prado, S. Alepuz, J. Bordonau, J. Nicolas-Apruzzese, P. Cortés and J. Rodriguez, "Model Predictive Current Control of Grid-Connected Neutral-Point-Clamped Converters to Meet Low-Voltage Ride-Through Requirements," in *IEEE Transactions on Industrial Electronics*, vol. 62, no. 3, pp. 1503-1514, March 2015.

[14] R. Vargas, P. Cortes, U. Ammann, J. Rodriguez and J. Pontt, "Predictive Control of a Three-Phase Neutral-Point-Clamped Inverter," in *IEEE Transactions on Industrial Electronics*, vol. 54, no. 5, pp. 2697-2705, Oct. 2007.

[15] S. Busquets-Monge, J. Bordonau, D. Boroyevich and S. Somavilla, "The nearest three virtual space vector PWM - a modulation for the comprehensive neutral-point balancing in the three-level NPC inverter," in *IEEE Power Electronics Letters*, vol. 2, no. 1, pp. 11-15, March 2004.

[16] P. Cortes, G. Ortiz, J. I. Yuz, J. Rodriguez, S. Vazquez and L. G. Franquelo, "Model Predictive Control of an Inverter With Output LC Filter for UPS Applications," in *IEEE Transactions on Industrial Electronics*, vol. 56, no. 6, pp. 1875-1883, June 2009.

[17] J. Pou, R. Pindado, D. Boroyevich and P. Rodriguez, "Evaluation of the low-frequency neutral-point voltage oscillations in the three-level inverter," in *IEEE Transactions on Industrial Electronics*, vol. 52, no. 6, pp. 1582-1588, Dec. 2005.